CONVECTIVE HEAT TRANSFER OVER A WALL MOUNTED CUBE AT DIFFERENT ANGLE OF ATTACK USING LARGE EDDY SIMULATION

by

Habibollah HEIDARZADEH, Mousa FARHADI*, and Kurosh SEDIGHI

Faculty of Mechanical Engineering, Babol University of Technology, Babol, Iran

Original scientific paper
DOI: 10.2298/TSCI110614088H

Turbulent fluid flow and convective heat transfer over the wall mounted cube in different flow angle of attack have been studied numerically using large eddy simulation. Cube faces and plate have a constant heat flux. Dynamic Smagorinsky-subgrid scale model were used in this study. Angles were in the range $0 \le \theta \le 45°$ and Reynolds number based on the cube height and free stream velocity was 4200. The numerical simulation results were compared with the experimental data of Nakamura et al. Characteristics of fluid flow field and heat transfer compared for four angles of attack. Flow around the cube was classified to four regimes. Results was represented in the form of time averaged normalized streamwise velocity and Reynolds stress in different positions, temperature contours, local and average Nusselt number over the faces of cube. Local convective heat transfer on cube faces was affected by flow pattern around the cube. The local convective heat transfer from the faces of the cube and plate are directly related to the complex phenomena such as horse shoe vortex, arch vortexes in behind the cube, separation and reattachment. Results show that overall convective heat transfer of cube and mean drag coefficient have maximum and minimum value at $\theta = 0$ and $\theta = 25°$, respectively.

Key words: *wall mounted cube, heat transfer, large eddy simulation, angle of attack*

Introduction

Flow over a wall mounted cube generates complex, unsteady and 3-D phenomena such as separation, reattachment, horseshoe vortex and arch-shaped vortexes. These phenomena effect on turbulence intensity, convective heat transfer and other fluid flow characteristics. As different flow phenomena are occurred on each face of cubes, therefore convective heat transfer is expected to be different by cube faces. 3-D roughness elements in the shapes of cube, diamond, and pyramid have long been considered for increasing heat transfer from a heat-exchanger surface. Flow around vehicles and building are other engineering application of flow around a 3-D obstacle. By changing the flow angle of attack, the flow pattern around the cube changes. So these changes effects on flow characteristics, turbulence intensity and convective heat transfer. Optimal angle can be identified for particular aim such as cooling of electronic equipment.As flow around a wall mounted cube has complex phenomena, a suitable numerical simulation should be employed to simulate the flow and heat transfer. Because of these complexities and the presence of large unsteady structures, RANS (Reynolds averaged Navier-Stokes) methods have considerable difficulties in predicting such flows. Also RANS methods

*Corresponding author; e-mail: mmahmoodi46@gmail.com

cannot simulate flow and heat transfer near the walls correctly. Direct numerical simulation (DNS) and large eddy simulation (LES) are more suitable methods for simulating such a complex and unsteady phenomena. In the LES method large eddies are resolved, while the small eddies are modeled by means of a subgrid eddy-viscosity model. In the present work, a dynamic Smagorinsky (DS) subgrid scale model was employed to solve the flow field and heat transfer around the wall mounted cube. Many studies have been done about fluid flow and convective heat transfer around wall mounted cube experimentally and numerically. In these studies complex phenomena and effect of them on fluid flow characteristics and local and average convective heat transfer around cube were investigated. Igarashi [1] studied experimentally effect of flow angle of attack on heat transfer from a square prism to an air stream. In this study angles of attack were in the range $0 \le \theta \le 45°$. He found that by changing the flow's angle of attack, the flow phenomena and patterns around the square prism changed. On its turn, this has resulted on the distribution of local Nusselt number to be also affected. Igarashi [2] experimentally studied local heat transfer from a square prism to an air stream. In this study he showed that flow pattern around square prism divided into four groups: (1) perfect separation and symmetric flow, (2) perfect separation an asymmetric flow, (3) reattachment flow, and (4) wedge flow. Also Natarajan and Chyu [3] experimentally studied effect of flow angle of attack on the local heat and mass transfer from a wall mounted cube. In their study Reynolds number was $8.2 \cdot 10^4$. They classified the flow pattern around the wall mounted cube into four different regimes; based on the flow features on face 4 (fig. 3). Meinders *et al*. [4] experimentally studied the local convective heat transfer from a wall mounted cube in turbulent channel flow. They studied distribution of local convective heat transfer around the cube and found that the complex vortex structure around the cube, in particular at the top and side faces, cause large variation in the local convective heat transfer. Meinders and Hanjalic [5] experimentally studied the vortex structure and heat transfer in turbulent flow over a wall mounted matrix of cubes. Nakamura *et al.* [6] investigated external flow around cubic obstacle. They studied the fluid flow and local heat transfer around a wall mounted cube on a flat plate turbulent boundary layers, and the effect of flow pattern such as flow separation and flow reattachment on the convective heat transfer. In [7] results of the experimental investigationof the fluid flow and local heat transfer around a wall mounted cube at 45° to the flow on a flat plate turbulent boundary layers, are given. By studying flow pattern on faces of cube and base plate, they showed that location of separation and reattachment are different toward the case $\theta = 0$. Niceno *et al.* [8] studied numerically the dynamics of flow and heat transfer on an internally heated multilayered matrix of cubes mounted on one of the walls of a plane channel using LES. Detailed information was obtained about the instantaneous and averaged velocity and temperature in the fluid around the cube, as well as the temperature and heat transfer on the cube surfaces. In addition, the simulation provided details about to the vortical structures and turbulence field around the cube and their relationship with the cube surface heat transfer. Farhadi and Rahnama [9] investigated flow over a wall mounted cube by LES.Effects of Reynolds number on flow over a wall mounted cube in a channel, was investigated by Sedighi and Farhadi [10]. Their results showed that the flow with higher Reynolds number has a shorter reattachment length. Flow over 3-D bodies *e. g*. square prism and sphere reported in [11, 12].Sohankar [13] also studied the flow over a bluff body from moderate to high Reynolds numbers using LES. Martinuzzi and Havel [14] and Farhadi and Sedighi [15] investigated the flow over two tandem wall mounted cubes experimentally and numerically, respectively. Lammers *et al.* [16] investigated a turbulent channel flow, with regularly spaced 2-D roughness elements mounted at the wall and perpendicular to the flow direction. They studied on the effect of elements mounted at the wall on the streamwise and the spanwisevelocity fluc-

tuations near the wall. Chakrabarty and Brahma [17] also experimentally studied effect of wall proximity in fluid flow and heat transfer from a square prism placed inside a wind tunnel. Their results showed that the values of average Nusselt number for all angles of attack, Reynolds numbers, and blockage ratios decrease as the prism moves in the direction of the upper wall of the wind tunnel. Hemida *et al.* [18] investigated the influence of attaching vortex generators to a surface of a heated cube on flow structures and heat transfer. Omidyeganeh and Abedi [19] numerically studied the wind flow around a cube in channel using large eddy simulation for turbulent flow. Noorullahi *et al.* [20] compared different semi dynamic subgrid scale models for large eddy simulation in a wall mounted cube. Their results show that these semi dynamic models could improve the ability of numerical simulation in comparison with other models witch use a constant coefficient for simulation of subgrid scale viscosity. Schmidt and Thiele [21] compared the results of DES with LES on flow over wall mounted cube at different RANS models. SeetaRatnam and Vengadesan [22] investigated of flow and heat transfer over wall mounted cube with several RANS models.

In the present study, effect of flow angle of attack on flow structure and heat transfer rate over a wall mounted cube on a flat plate in the turbulent boundary layers was investigated numerically. The flow angles of attack are in the range $0 \le \theta \le 45°$. These angles are $\theta = 0$, 10°, 25°, and 45°. Local and average convective heat transfer, were studied on faces of cube at different angles.

Mathematical model

Turbulent flow over obstacle is modeled by LESin which the larger 3-D unsteady turbulent motions are directly represented, whereas the effect of small scales of motion is modeled. To do this, a filtering operation is introduced to decompose the velocity vector, u_i into the sum of a filtered (or resolved) component, $\overline{u}_i$ and a residual (or subgrid scale, SGS) component u_i'. This operation can be represented with a filter of width Δx such that convolution of any quantity $f(x_i, t)$ by the filter function $G_{\Delta x}(x_i)$ is in the form:

$$\overline{f}(x_i,t) = \overline{f}(y_i,t) G_{\Delta x}(x_i)(x_i - y_i)\mathrm{d}y_i, \quad f' = f - \overline{f} \tag{1}$$

The equations for the evolution of the filtered velocity filed are derived from the Navier-Stokes equations. These equations are of the standard form, with the momentum equation containing the residual stress tensor. Application of the filtering operation to the continuity and Navier-Stokes equations gives the resolved Navier-Stokes equations, which, in nondimensional incompressible form, are equations:

$$\frac{\partial \overline{u}_i}{\partial \overline{x}_i} = 0 \tag{2}$$

$$\frac{\partial \overline{u}_i}{\partial t} + \frac{\partial}{\partial x_j}(\overline{u}_i \overline{u}_j) = -\frac{1}{\rho}\frac{\partial \overline{p}}{\partial x_i} + \nu \frac{\partial^2 \overline{u}_i}{\partial x_j x_j} - \frac{\partial \tau_{ij}}{\partial x_j} \tag{3}$$

$$\frac{\partial \overline{T}}{\partial t} + \frac{\partial (\overline{u}_i \overline{T})}{\partial x_i} = \frac{\partial}{\partial x_j}\left(\alpha \frac{\partial \overline{T}}{\partial x_j} - h_j\right) \tag{4}$$

where $\overline{P}$ is the pressure, and $\overline{u}_1$, $\overline{u}_2$, and $\overline{u}_3$ are the streamwise, cross-stream, and spanwise components of velocity, respectively. These govern the dynamics of the large, energy-carrying scales of motion. Reynolds number is defined as, $U_{\text{inlet}}H/\nu$ where U_{inlet} and H are the inlet veloc-

ity of entrance profile and cube height, respectively. The effect of small scales upon the resolved part of turbulence appears in the SGS stress term as eq. (5) which must be modeled:

$$\tau_{ij} = \overline{u_i u_j} - \overline{u}_i \overline{u}_j \tag{5}$$

The main effect of the SGS stresses is dissipative around the cut-off spectrum, *i. e.* to withdraw energy from the part of the spectrum that can be resolved. One model for the SGS stress term τ_{ij} is based on its dependence on the filtered strain rate through an eddy viscosity given by:

$$\tau_{ij} = 2\nu_{\mathrm{SGS}}\overline{S}_{ij} + \frac{1}{3}\tau_{kk}\delta_{ij} \tag{6}$$

where $\overline{S}_{ij}$ is the resolved strain rate given by:

$$\overline{S}_{ij} = \frac{1}{2}\left(\frac{\partial \overline{u}_i}{\partial x_j} + \frac{\partial \overline{u}_j}{\partial x_i}\right) \tag{7}$$

where ν_{SGS} is the SGS eddy-viscosity.

The modified SGS heat fluxes h_j are defined as:

$$h_j = \overline{u_j T} - \overline{u}_j \overline{T} \tag{8}$$

The modified SGS heat fluxes h_j are modeled by the eddy-diffusivity hypothesis with constant turbulent Prandtl number, Pr_t, as:

$$h_j = -\frac{\nu_{\mathrm{SGS}}}{\mathrm{Pr}_t}\frac{\partial \overline{T}}{\partial x_j} \tag{9}$$

In this study, we have $\mathrm{Pr}_t = 0.85$.

Subgrid scale model

In this study, we used DS subgrid scale model for modeling of SGS eddy viscosity. This model was first proposed by Smagorinsky. In this model, the eddy viscosity is modeled by:

$$\nu_{\mathrm{SGS}} = L_s^2 \left|\overline{S}\right| \tag{10}$$

where L_s is the mixing length for subgrid scales and $\left|\overline{S}\right|$ is given by:

$$\left|\overline{S}\right| = \sqrt{2\overline{S}_{ij}\overline{S}_{ij}} \tag{11}$$

L_s is computed using:

$$L_s = \min\left(\kappa r, C_s V^{\frac{1}{3}}\right) \tag{12}$$

where κ is the von Karman's constant, r – the normal distance to the closest wall, and V – the volume of the computational cell. In this study $\kappa = 0.4187$ and C_s is the Smagorinsky constant. In the Smagorinsky model, C_s value usually is around 0.1 but Germano *et al.* [23] and subsequently Lilly [24] conceived a procedure in which the Smagorinsky model constant, C_s, is dynamically computed based on the information provided by the resolved scales of motion. The dynamic procedure thus obviates the need for users to specify the model constant C_s in ad-

vance. The C_s is obtained using the dynamic Smagorinsky model varies in time and space over a fairly wide range. More detail can be found in [25].

Numerical method and boundary condition

In this study, the commercial CFD software FLUENT 6.3 was used for simulation that was based on finite volume method. Associated preprocessor GAMBIT 2.2 was used for the construction of the computational grid. FLUENT uses a control-volume-based technique to convert a general scalar transport equation to an algebraic equation that can be solved numerically. This control volume technique consists of integrating the general scalar transport equation about each control volume that yields a discrete equation on each control-volume. In this software, pressure-based solver was used to solve discrete equations. The pressure-based solver uses a solution algorithm where the governing equations are solved sequentially and segregated from one another. Because the governing equations are non-linear and coupled, the solution loop must be carried out iteratively in order to obtain a converged numerical solution.

An important issue in the LES computations is that using at least second orders accuracy of both time and spatial discretization of the equations. Linear equations system that was yielded from discretization of equations was solved by using an implicit linear equation solver (Gauss-Seidel) in conjunction with an algebraic multi-grid (AMG) method. SIMPLE (semi implicit method for pressure linked equation) algorithm was used for coupling the pressure and velocity terms. Second-order-accurate bounded central-differencing scheme by Leonard [26] is used for spatial discretization of convection terms in governing equations. The QUICK and central-differencing scheme has some deficiencies in comparison with the bounded central-differencing scheme. Central-differencing scheme often leads to unphysical oscillations in the solution fields and QUICK scheme has numerical dissipation. For spatial discretization of diffusion terms central-differencing scheme that is second-order accurate was used. A second-order implicit scheme was used for temporal discretization of governing equations and all equations solved by iterative time-advancement (ITA) method in a time step. The time step $\Delta t$was set to 10^{-3}s and kept constant during the simulation. The total of simulation time continued to time that flow becomes statically steady. The total time in the simulation was 65000 time steps. It was founded from time history of some flow average parameters, for example velocity. The simulation continued until the flow average parameter becomes steady.

The grid is finer near the surface of the cube in all directions and near the plate. In LES for getting good results, height of the first cell near walls should be achieved from $y^+ = 1$. $y^+$is:

$$y^+ = \frac{u^* y}{\nu}, \quad u^* = \sqrt{\frac{\tau_0}{\nu}} \tag{13}$$

In this study we used $y^+ = 1$ for the first cell in near walls. The minimum grid spacing used in the present computations is0.0075H in x-direction, 0.0085H in y- and z-direction with a grid expansion ratio of 1.05.The number of grid points used in the present computations were161 × 86 × 144 in the x-, y-, and z-direction, respectively.The geometry considered in this study consists of a surface mounted cube with a uniform velocity at the inlet, fig. 1(a). Orientation of cube is counter clockwise and faces are shown on top view, fig. 1(b). The streamwise, normal and spanwise lengths of the computational domain are 11H, 5H, and 7H, respectively. The inlet profile was chosen according to the experimental study of Nakamura *et al.* [6, 7]. Uniform flow is therefore imposed at the inlet of the computational domain. So the spanwise and upside boundary condition was selected symmetry. The free-stream turbulence

intensity was about 0.5% .The no-slip boundary conditions were used for all the walls. The outlet boundary condition is of convective type for a quantity ϕ is:

$$\frac{\partial \phi}{\partial t} + U_b \frac{\partial \phi}{\partial n} = 0 \tag{14}$$

Such convective boundary condition is capable of predicting unsteady flow behavior at the exit with good accuracy. The upside boundary condition was selected symmetry. Surfaces of cube and plate have wall boundary condition. Surfaces of cube and plate were under condition of constant heat flux. The Reynolds number was 4200.Also the Prandtl number in this study was 0.72.

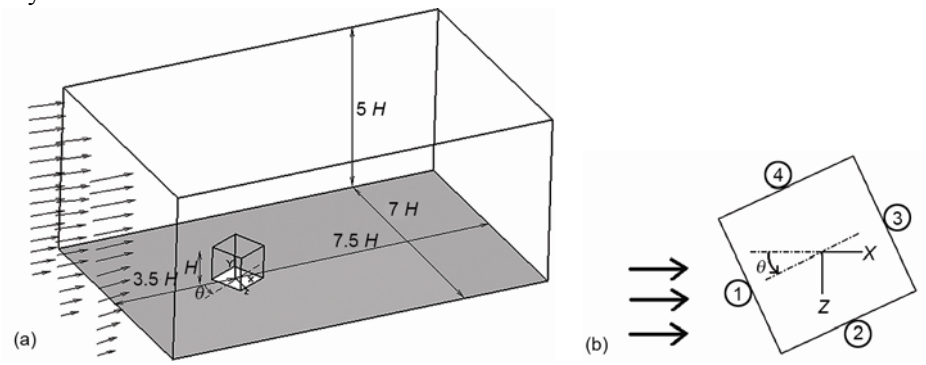

Figure 1. (a) Geometry of problem, (b) top view of cube

Results

Turbulent flow over the wall mounted cube has complex phenomena such as horse shoe vortex, arch-shaped vortexes, recirculation zones, flow separation, and reattachment (figs. 4 and 5). When fluid passes over the cube, variables such as velocity and pressure affect these complex phenomena and in turn influence turbulence intensity, convective heat transfer, and other fluid flow characteristics. Orientation of cube and variation of flow attack angle influence the flow characteristics and heat transfer around the cube. In this study 3-D LES was carried out to solve fluid flow and convective heat transfer around the wall mounted cube. The study was carried out for four angles of attack. As it can be seen from fig. 2 all flow phenomena that were formed on experimental study can be detected by numerical considerations. These phenomena are horseshow vortexes (*H*), arch vortexes (*A*), recirculation zone in behind the cube (*R*), vortexes near side (*L*) and top faces (*T*), and vortexes in upstream (*F*) and downstream (*B*) of cube. These phenomena can be seen in fig. 3.

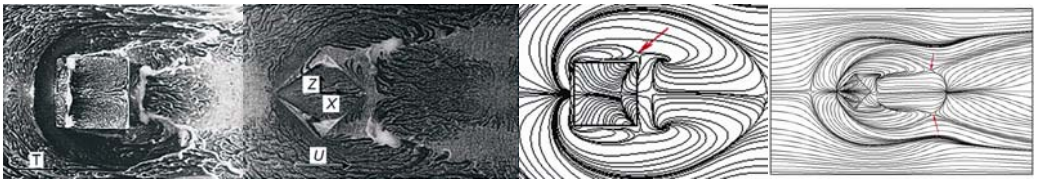

(a) (b)

Figure 2. Time averaged streamlines at top view for θ = 0 (left) and θ = 45 (right), (a) experimental data [6, 7], and (b) present study

Time averaged streamlines on all faces for four angles of attack are shown in fig. 4. It can be seen that flow features are not similar on face 4 at different angles of attack. Therefore flow is classified to four regimes based on the features on face 4.This classification is shown in tab. 1.This was also reported by Natarajan and Chyu [3]. Figure 4 also indicated the effect of angle of attack on all faces of cube as it is illustrated at $\theta = 0$.

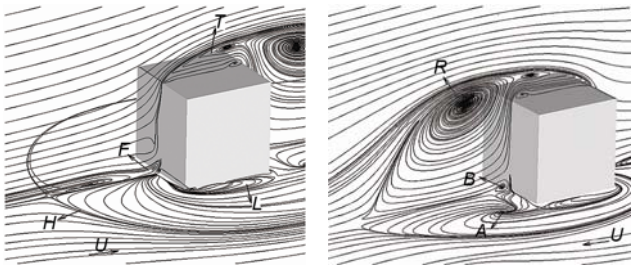

Figure 3. Complex phenomena around the cube (y = 0 and z = 0 planes)

Table 1. Flow regimes classification at different angle of attack

Angle (θ)	0°	10°	25°	45°
Flow regimes	Perfect separation and symmetric flow	More separation, less reattachment and asymmetric flow	More reattachment, less separation and asymmetric flow	Wedge flow

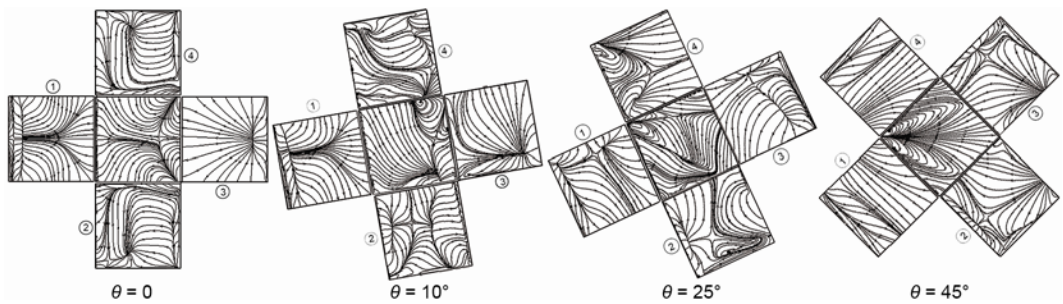

Figure4. Time averaged streamlines on cube faces at different angle of attack

In $\theta = 0$, faces 4 and top lie into separation region. In $\theta = 10°$, most part of these faces lie into separation region. In $\theta = 25°$ flow separated from the upstream edge of face 4 reattaches on most parts of this face. In $\theta = 45°$ a wedge-type behavior of the flow appears on faces4 and 1 and the disappearance of separation phenomenon from face 4, happens. In all flow regimes face 2 lies in the separation region. Time averaged streamlines on top face in $\theta = 25°$ show that the flow pattern is formed of different flow structures such as recirculation. At $\theta = 45°$ on top face, flow is reattached in near junction of faces 2 and 3.

Time averaged streamlines on top view (left) and symmetry plane (z = 0) (right) for $0 \le \theta \le 45°$ are shown in fig. 5. Separation region behind the cube has high turbulent intensity, by increasing of flow attack angle, this region become larger. At larger angles, recirculation region on top face has shorter length. Horseshoe vortex, two small recirculation regions in near front and rear of cube, typical converging-diverging behavior of horse shoe vortex and arch-shaped vortexes in behind the cube were common in all angles of attack. The saddle points on the plate for all angle of attack are indicted with arrows in fig. 5. Some complex flow phenomena that are mentioned above can observe clearly in fig. 6.

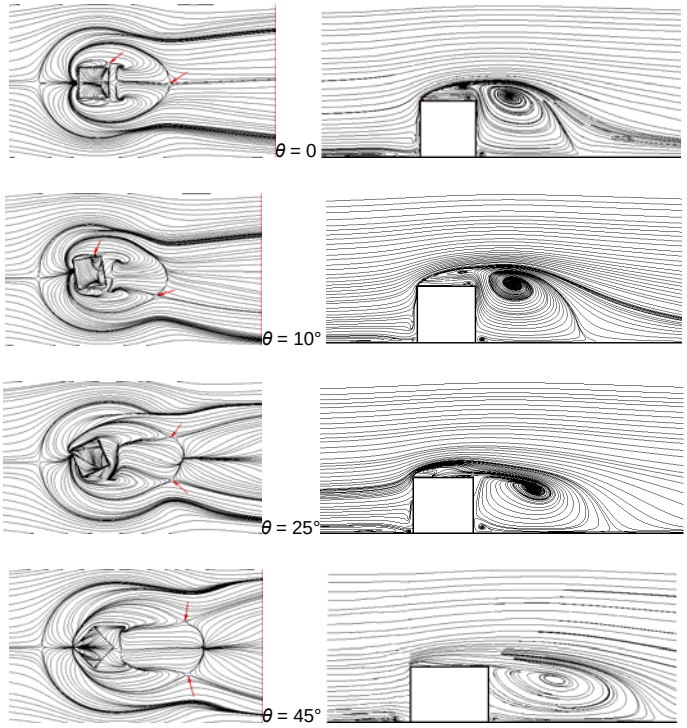

Figure 5. Time averaged streamlines on top view (left) and symmetry plane (z = 0) (right)

Figure 6. Time averaged streamlines around a wall mounted cube (for color image see journal web-site)

Turbulence intensity is affected by formation of complex flow phenomena in the top and rear region of the cube. Therefore velocity, Reynolds stress and their variation are changed in different positions at these regions (x = 0, $x = H$, $x = 2H$, and $x = 3H$ on symmetry plane z = 0). Figures 7and8 show the normalized time averaged streamwise velocity $\overline{U}/U_b$ and the normalized time averaged Reynolds stress $\overline{u'v'}/U_b^2$ for different angle of attack. It is indicated that variation of Reynolds stress and velocity profile due to high turbulence intensity is high. Figure 7 also indicated at $y/H > 1$ time averaged streamwise velocity gradient is acceded to zero; therefore turbulence properties value decrease to zero. At higher angle of attack time averaged streamwise velocity gradient approached to zero at smaller y/H. Due to high velocity and turbulent viscosity and lack of separation region at x = 0 in $\theta = 45°$, the maximum Reynolds stress magnitude is higher in comparison to the other angle of attack (fig. 8). In $x = H$ increase on θ causes a decrease on the maximum Reynolds stress magnitude. But at greater position ($x = 3H$) the result is *vice versa*.

As it can be observed from fig. 9 mean drag coefficient is decreased approximately 25% by increasing angle of attack until $\theta = 25°$. This is due to large low pressure region at smaller angle. Further increase in θ causes a slight increase in mean drag coefficient due to approach to symmetry condition. Drag coefficient is defined as eq. (15) that $\vec{F}_a$ is total force component, $\vec{F}_p$ is pressure force component, $\vec{F}_v$ is total force component, $\vec{a}$ is specified force vector, ρ is density, u is velocity, and A is area:

$$C_d = \frac{\vec{F}_a}{\frac{1}{2}\rho u^2 A} \tag{15}$$

$$\vec{F}_a = \vec{a}\,\vec{F}_p + \vec{a}\,\vec{F}_v \qquad (16)$$

Mean drag coefficient is defined as:

$$\overline{C_d} = \frac{1}{t}\int_0^t C_d\,\mathrm{d}t \qquad (17)$$

Heat transfer

Dimensionless mean temperature (T^*) contour over the plate in different flow angle of attack is plotted in fig. 10. The horse shoe vortex in the upstream and recirculation region at the rear of the cube make mixing in the flow field, therefore the heat transfer increase and mean temperature is low in these regions. At bigger angle these regions increase. By increasing angle of attack, turbulence intensity decreases in downstream of cube near rear faces so convective heat transfer

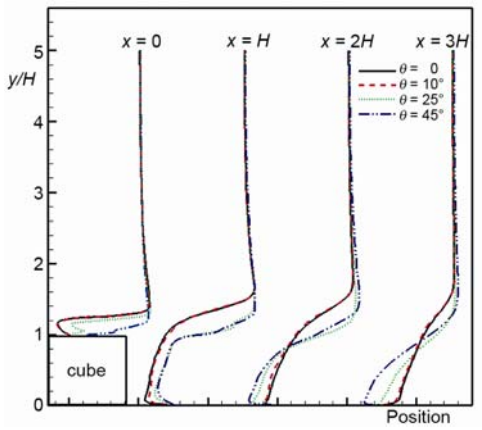

Figure 7. The normalized time averaged streamwise velocity profile ($\bar{U}/U_b$) for different angle of attack at different positions on z = 0 plane (for color image see journal web-site)

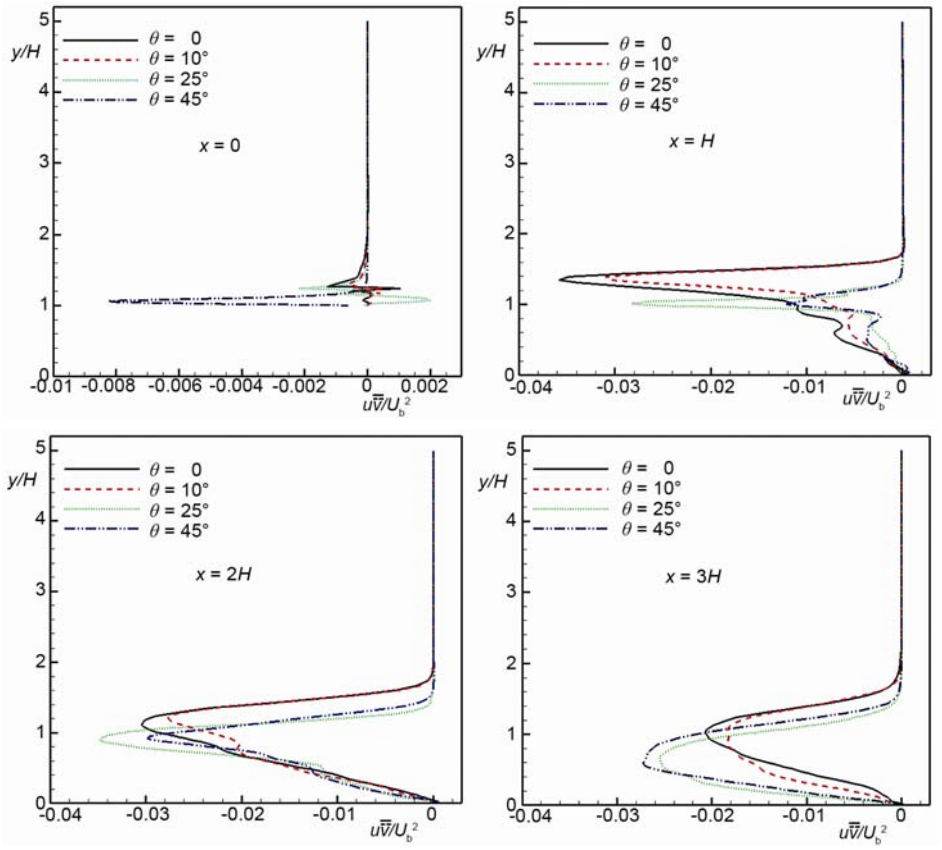

Figure 8. The normalized time averaged Reynolds stress ($\overline{u'v'}/U_b^2$) for different angle of attack at different positions on z = 0 plane (for color image see journal web-site)

decreases and mean temperature increases. From fig. 10 it can be seen that a high temperature region is formed near face 2 due to small recirculation region. Temperature magnitude is high at large θ. Any increase on θ near face 4 causes a reduction on recirculation region size and at θ = 45°, recirculation becomes disappear. This caused mean temperature decreases as the angle of attack increases.

Time average Nusselt number is defined as eq. (18) that H and k_f are, cube height and thermal conductivity of fluid, respectively:

$$\overline{\mathrm{Nu}} = \frac{1}{t}\int_0^t \mathrm{Nu}\,\mathrm{d}t \tag{18}$$

$$\mathrm{Nu} = \frac{q''H}{k_f(T_s - T_{bi})} \tag{19}$$

Mean Nusselt number is also defined as:

$$\mathrm{Nu_m} = \frac{1}{H}\int_0^H \overline{\mathrm{Nu}}\,\mathrm{d}t \tag{20}$$

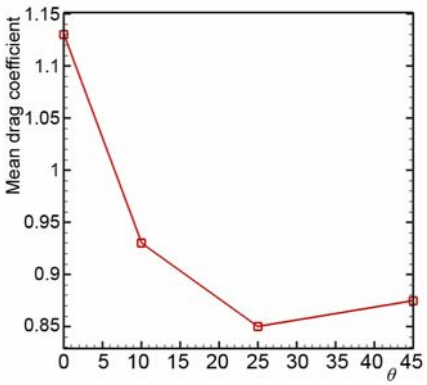

Figure 9. Mean drag coefficient for different angle of attack

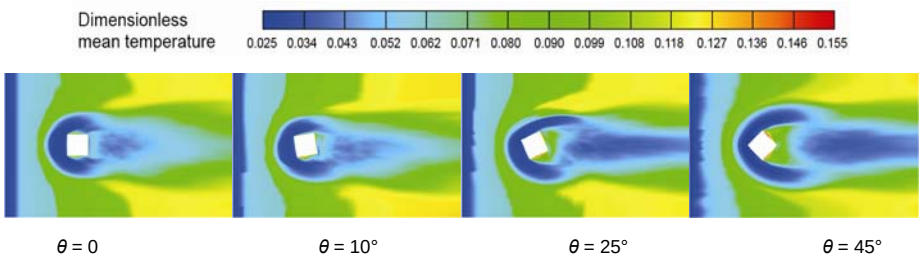

Figure 10. Dimensionless mean temperature contour over the plate for different angle of attack (for color image see journal web-site)

Here q'', T_s and T_{bi} are the heat flux, the surface temperature and the inlet bulk temperature, respectively. A good accuracy was observed in comparison of numerical and experimental results [6, 7] on convective heat transfer (fig. 11).

For study of the local convective heat transfer, time average local Nusselt number was considered for four angles of attack on cube faces. Results were shown in the contour form (fig. 12).

(a) For θ = 0. On the face1 in stagnation point fluid flow velocity is zero and increases by approaching to edges. It can be seen in figs. 11 and 12, convective heat transfer increases by approaching to edges and the Nusselt number has maximum value in near edges. Also it can be seen in fig. 12 that on the face1 the Nusselt number distribution is almost flat along the vertical direction except near the upper and bottom parts. Nusselt number variation, on faces 2, 4 and top is higher than other faces due to these faces lie in separation region. On these faces the Nusselt number at separation points has minimum value

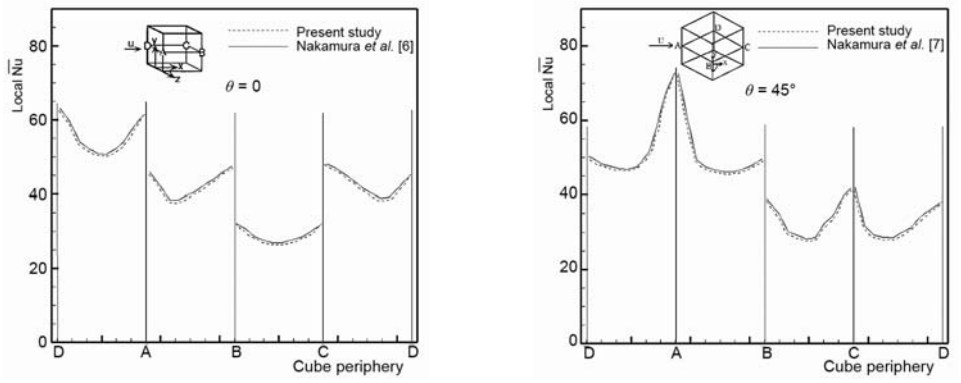

Figure 11. Comparison of time average local Nusselt number distributions with experimental data [6, 7]

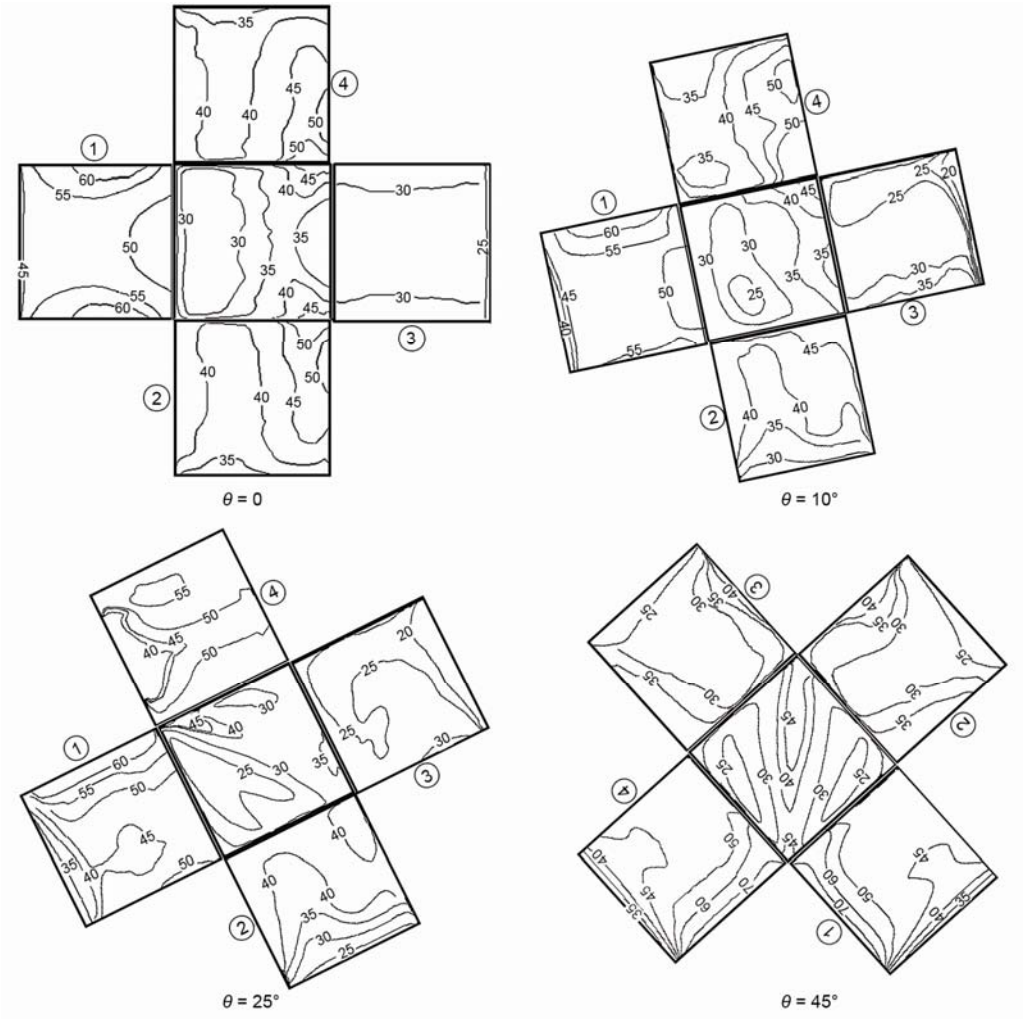

Figure 12. Time average local Nusselt number contours on cube faces at different angle of attack

and increases to the backward edges. Near the backward edges faces 2 and, 4 the values of Nusselt number in the upper part are higher than those in the bottom part. Transport phenomena downstream the cube near face 3 greatly is influenced by the arch-shaped vortexes. Slow-moving fluid near this face induces lower Nusselt values in comparison with the other faces. The result showed a small variation on local Nusselt number on the face 3 along the horizontal direction and the variation is become greater in near edges.

(b) For $\theta = 10°$. As it is mentioned before, flow pattern on faces of cube at $\theta = 10°$ is asymmetry. So as a result, convective heat transfer on faces of cube is asymmetry. On face1, stagnation point shifts slightly toward the upper left hand corner (near junction of face4). Similar to $\theta = 0$, convective heat transfer increases approaching to edges and the Nusselt number has maximum value in near edges. As it can be observed from fig. 12, on face1 Nusselt number has minimum value in bottom part. In this angle Nusselt number distribution on face2 is similar to $\theta = 0$. On face 4 convective heat transfer in reattachment region (near downstream edge) and in separation region (near upstream edge) is greater and less than other parts, respectively. By approaching to downstream edge, Nusselt number increased in this face. Also Nusselt number distribution on top face is asymmetry due to the reattachment phenomenon happen in downstream left hand corner (near junction of face 4).Therefore a maximum Nusselt number value is obtained in this region(fig. 12). It can be seen that at the face3 of cube Nusselt number distribution is different with that observed in $\theta = 0$.As Arch-shaped vortexes behind the cube are asymmetry and they shift slightly toward junction edge of face 2 (fig. 5).On face 3 Nusselt number increases by approaching to junction edge of face 2 but decreases as approaching to junction edge of face 4.

(c) For $\theta = 25°$. A similar asymmetry condition for convective heat transfer of faces of cube was observed as $\theta = 10°$. As it can be obtain from fig. 4, stagnation point on face1 shifts more toward junction edge of face 4. In this face Nusselt number by approaching to junction edge of face 2 decreases due to the development of a thermal boundary layer. Nusselt number distribution on face2 is similar to $\theta = 0$ and 10°. As it is mentioned before, more parts of face 4 lie in reattachment region. So Nusselt number is high in more parts of this face, but its value near upstream edge that lies in separation region is rather low. It can be seen from fig. 4 at $\theta = 25°$ two arch-shaped vortexes form with different sizes in behind and more apart from the cube, as convective heat transfer from face 3 decreases. Nusselt number in face 3 is almost uniform and in near junction edge of face 2 is a slightly more than other part of this face.

(d) For $\theta = 45°$. On front (1and 4) faces, Nusselt number in near upstream edge has maximum value and by approaching to downstream edge decreases due to the development of a thermal boundary layer. Nusselt number distribution on rear (2 and 3) faces is similar to face 2 in other angles. Figure 12 shows that Nusselt number on top face in central part, near junction of front (1 and 4) faces and near junction of rear (2 and 3) faces, is rather high. In other parts that lie in separation region Nusselt number is low.

Mean Nusselt number is used for comparison convective heat transfer at cube and each faces of cube at different angle of attack (fig. 13). The mean Nusselt numbers for faces 1, 3 and top show a similar trend as θ increases. Among five faces, faces 4 and 2 have strongest dependence of mean Nusselt number on the magnitude of θ. By increasing angle of attack mean Nusselt number at face 4 increases.As this face is lies on separation region at smaller angles. By increasing angle of attack mean Nusselt number at face 2 decreased due to a bigger angles this face influenced by the arch-shaped vortexes. Side faces (2 and 4) at $\theta = 0$ have

similar mean Nusselt number value due to they lie in symmetry condition. Also this occurs at $\theta = 45°$ in front (1 and 4) and rear (2 and 3) faces. Variation of overall Nusselt number of cube with angle of attack is shown in fig. 14. Overall Nusselt number of cube has maximum value at $\theta = 0$ and it is decreased approximately 12% by increasing angle of attack until $\theta = 25°$. This reduction is due to difference of flow pattern and phenomena around the cube that illustrated before. Farther increase in $\theta°$ causes approximately 11.5% increases in this value. This shows that overall convective heat transfer from cube is more in symmetry in compare to asymmetry cases. Also in this figure overall Nusselt number in cases $\theta = 0$ and 45° compared with experimental results of Nakamura *et al.* [6, 7]. The numerical simulation results show a good accuracy in comparison with the experimental data.

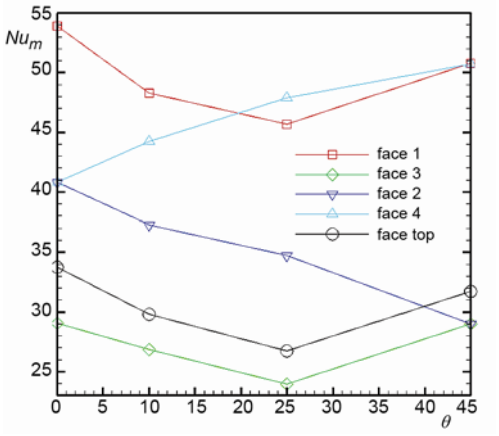

Figure 13. Mean Nusselt number on cube faces for different angles
(for color image see journal web-site)

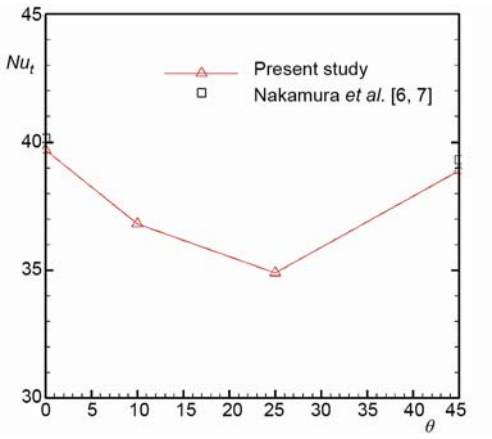

Figure 14. Overall Nusselt number of cube for different angles
(for color image see journal web-site)

Conclusions

The 3-D simulation of the turbulent flow field and convective heat transfer over a wall mounted cube in different flow angle of attack were done by LES. Complex phenomena such as horse shoe vortex, arch-shaped vortexes, separation and reattachment form around the cube that effect on fluid flow characteristics and heat transfer. Four flow regimes around a wall mounted cube in different angle of attack was considered due to different flow features on face 4. This classification was: (a) perfect separation and symmetric flow ($\theta = 0$), (b) more separation, less reattachment and asymmetric flow ($\theta = 10°$), (c) more reattachment, less separation and asymmetric flow ($\theta = 25°$), and (d) wedge flow ($\theta = 45°$). Time averaged Reynolds stress and velocity, have strong variation in the separation regions behind and top of cube. By increasing distance from the cube in streamwise direction, maximum Reynolds stress magnitude was high in bigger angle of attack. By increasing angle of attack, mean temperature in recirculation regions near faces 3 and 4 increases and decreases, respectively. The local convective heat transfer from the faces of cube and plate to the fluid is directly related to the complex phenomena. On all cube faces local convective heat transfer in separation and reattachment regions is low and high respectively. Arch-shaped vortexes in behind the cube cause uniform convective heat transfer on rear face. The highest overall Nusselt number and mean drag coefficient for cube are obtained in $\theta = 0$ and the lowest in $\theta = 25°$.

Nomenclature

A – area, [m^2]
$\vec{a}$ – specified force vector, [−]
C_s – Smagorinsky constant, [−]
C_d – drag coefficient, [−]
$\overline{C_d}$ – mean drag coefficient, [−]
$\vec{F}_a$ – total force component, [N]
$\vec{F}_p$ – pressure force component, [N]
$\vec{F}_v$ – viscous force component, [N]
H – cube height, [m]
k_f – fluid thermal conductivity, [WK^{-1}m^{-1}]
Nu − Nusselt number [$= q''H/k_f(T_s - T_{bi})$], [–]
$\underline{\mathrm{Nu}}_t$ – overall Nusselt number, [–]
$\overline{\mathrm{Nu}}$ – time average Nusselt number, [–]
Nu_m – mean Nusselt number, [–]
P – pressure, [kgs^{-1}m^{-1}]
Pr_t – turbulent Prandtl number, [–]
Pr – Prandtl number (= ν/α), [−]
q'' – heat flux, [wm^{-2}]
Re − Reynolds number (= $U_{inlet}H/\nu$), [–]
r − normal distance, [m]
S − strain rate, [−]
T_{bi} − inlet bulk temperature, [K]
T_m − mean temperature, [K]
T_s − surface temperature, [K]
T^* − dimensionless mean temperature [$=(T_m - T_{bi})/(q'' H/k)$], [□]
t – time, [s]
U_b − bulk velocity, [ms^{-1}]
U_{inlet} – velocity at the entrance, [ms^{-1}]
v − volume, [m^3]
u − velocity, [ms^{-1}]
u^* − friction velocity, [ms^{-1}]
y^+ – normalized distance, [–]

Greek symbols

α − thermal diffusivity, [m^{2}s^{-1}]
δ_{ij} – Kronecker delta, [–]
θ – angle of attack, [deg]
κ – von Karman's constant, [–]
ν − kinematic viscosity, [m^{2}s^{-1}]
ρ − density, [kgm^{-3}]
τ − shear stress, [kgm^{-1}s^{-2}]

References

[1] Igarash, T., Heat Transfer from a Square Prism to an Air Stream, *Int. J. Heat Mass Transfer, 28* (1985), 1, pp. 175-181
[2] Igarash, T., Local Heat Transfer from a Square Prism to an Air Stream, *Int. J. Heat Mass Transfer, 29* (1986), 5, pp. 777-784
[3] Natarajan, V., Chyu, M.K., Effect of Flow Angle of Attack on the Local Heat/Mass Transfer from a Wall-Mounted Cube, *ASME J. Heat Transfer, 116* (1994), 3, pp. 552-560
[4] Meinders, E. R., *et al*., Experimental Study of the Local Convective Heat Transfer from a Wall Mounted Cube in Turbulent Channel Flow, *ASME J. Heat Transfer, 121* (1999), 3, pp. 564-573
[5] Meinders, E. R., Hanjalic, K., Vortex Structure and Heat Transfer in Turbulent Flow over Wall-Mounted Matrix of Cubes, *Int. J. Heat and Fluid Flow, 20* (1999), 3, pp.255-267
[6] Nakamura, H., *et al*., Local Heat Transfer around a Wall Mounted Cube in theTurbulent Boundary Layer, *Int. J. Heat and Mass Transfer, 44* (2001),18, pp. 3385-3395
[7] Nakamura,H., *et al*., Local Heat Transfer around a Wall Mounted Cube at 45° toFlow in a Turbulent Boundary Layer, *Int. J. Heat and Fluid Flow, 24* (2003), 6, pp.807-815
[8] Niceno, B., *et al*., Turbulent Heat Transfer from a Multi-Layered Wall Mounted Cube Matrix: a Large Eddy Simulation, *Int. J. Heat and Fluid Flow*, *23* (2002), 2, pp.173-185
[9] Farhadi, M., Rahnama, M., Large Eddy Simulation of Separated Flow over a Wall Mounted Cube,*ScientiaIranica*, *13* (2006), 2, pp. 124-133
[10] Sedighi, K., Farhadi, M., Three-Dimensional Study of Vortical Structure around a Cubic Bluff Body in a Channel, *FactaUniversitatisSeries: Mechanical Engineering*, *4* (2006), 1, pp. 1-16
[11] Bakic,V.,Experimental Investigation of a Flow Arounda Sphere, *Thermal Science*, *8* (2004), 1, pp. 63-81
[12] Bakic, V., *et al*., Experimental Investigation of Turbulent Structures ofFlow around a Sphere, *Thermal Science*, *10* (2006), 2, pp. 97-112
[13] Sohankar, A., Flow over a Bluff Body from Moderate to High Reynolds Numbers Using Large Eddy Simulation, *J .Computers & Fluids, 35* (2006), 10, pp. 1154-1168
[14] Martinuzzi, R. J., Havel, B.,Vortex Shedding from Two Surface Mounted Cubes in Tandem, *Int.J. Heat and Fluid Flow*, *25* (2004), 3, pp. 364-372
[15] Farhadi, M., Sedighi, K., Flow over Two Tandem Wall Mounted Cubes Using Large Eddy Simulation, *Proceedings of the Institution of Mechanical Engineers, Part C: Journal of Mechanical Engineering Science, 222* (2008), 8, pp. 1465-1475

[16] Lammers, P., *et al*., Numerical Experiments on Wall Turbulence at Low Reynolds Number, *Thermal Science*, *10* (2006), 2, pp. 33-62
[17] Chakrabarty, D., Brahma, R., Effect of Wall Proximity in Fluid Flow and Heat Transfer from a Square Prism Placed Inside a Wind Tunnel, *Thermal Science*, *11* (2007), 4, pp. 65-78
[18] Hemida, H., *et al*., Local Heat Transfer Enhancement around a Matrix of Wall Mounted Cubes Using Passive Flow Control: Large-Eddy Simulations, *Int. J. Heat and Fluid Flow*, *29* (2008), 5, pp. 1258-1267
[19] Omidyeganeh, M., Abedi, J., Numerical Simulation of the Wind Flow around a Cube in Channel, *6th International Colloquium on: Bluff Bodies Aerodynamics & Application,* Milano, Italy, 2008
[20] Nooroulahi, M., *et al.*, Large Eddy Simulation of Flow over a Wall-Mounted Cube: Comparison of Different Semi Dynamic Subgrid Scale Models, *Int. J. of Multi physics, 6* (2012), 1, pp.43-60
[21] Schmidt, S., Thiele, F., Comparison of Numerical Methods Applied to Flow over Wall-Mounted Cubes, *Int. J. Heat and Fluid Flow, 23* (2002), 3, pp. 330-339
[22] SeetaRatnam, G., Vengadesan, S.,Performance of Two Equation Turbulence Models for Prediction of Flow and Heat Transfer over a Wall Mounted Cube, *Int. J. Heat and Mass Transfer*, *51* (2008), 11, pp. 2834-2846
[23] Germano, M., *et al.*, A Dynamic Subgrid-Scale Eddy Viscosity Model, *Physics of Fluids A, 3* (1991), 7, pp. 1760-1765
[24] Lilly, D. K., A Proposed Modification of the Germano Subgrid-Scale Closure Model, *Physics of Fluids*, *4* (1992), 3, pp. 633-635
[25] ***, FLUENT, *Turbulence models*, Documentation report, Chapter 9
[26] Leonard, B. P., The Ultimate Conservative Difference Scheme Applied on Unsteady One-Dimensional Advection, *J. Computer Methods in Applied Mechanics and Engineering*, *88* (1991), 1, pp. 17-74

Paper submitted: June 14, 2011
Paper revised: February 20, 2013
Paper accepted: June 26, 2013